

ISOLA Code for Multiple-Point Source Modeling—Review



Jiří Zahradník and Efthimios Sokos

1 Introduction

ISOLA software package has been developed to invert local or regional full-wave seismograms for single- and multiple-point source models. The code was introduced in 2003; since then it has been continually upgraded, and, presently, it can be considered a well-established tool, used worldwide. Originally, the code name came from ‘isolated asperities’, to be resolved at fault planes of large earthquakes. However, with time, the code has been adapted for very diverse applications, ranging from Mw 0.3 to Mw 9. Many research papers based on usage of ISOLA have been published (see References). Almost every new application is challenging—hence the code is continually updated. The objective of this work is to explain the basic principles of the method, review code status, demonstrate a few examples to attract new users, and shortly touch also future development. The code is free, and can be downloaded together with manual and test examples from <http://seismo.geology.upatras.gr/isola/> (last accessed March 2018).

2 Basics

ISOLA software serves for modeling an extended seismic source as a point source, or a series of point sources. The point source contributions to an earthquake source model are called *subevents*. Their moment tensors (MT) are calculated by *least-squares*, using a full, deviatoric (i.e. zero-trace), or DC-constrained mode (i.e. requesting the double couple part to be close to 100%). Alternatively, 100% DC

J. Zahradník

Faculty of Mathematics and Physics, Charles University, Prague, Czech Republic

e-mail: jiri.zahradnik@mff.cuni.cz

E. Sokos (✉)

Seismological Laboratory, Department of Geology, University of Patras, Patras, Greece

e-mail: esokos@upatras.gr

focal mechanisms of the subevents can be kept fixed (prescribed), and inversion is performed only for position, time and moment of the subevents.

The position and time of subevents are calculated by a *space-time grid search*. The spatial grids are either linear or planar, e.g. along horizontal planes, or assumed fault planes. The subevent moment-rate time function, also called elementary time function is supposed to be known (delta function, or a single triangle of a prescribed duration). Alternatively, the time function can be calculated from waveform data, assuming a known focal mechanism. If a source appears (at low frequencies) as a single dominant subevent, we speak about centroid position and centroid moment tensor determination (CMT). The name centroid reminds that it is ‘center of gravity’ of slip on the fault. For small earthquakes, centroid and hypocenter are (within errors) identical.

Green’s functions, including near-, intermediate- and far-field terms, are calculated by the discrete wavenumber method (broadly used code AXITRA of Bouchon 1981 and Coutant 1989), using a 1D velocity model (parallel layers with constant parameters). In this way, all body waves and surface waves existing in the velocity model are automatically taken into account. Alternatively, several source-station, path-dependent, 1D models can be used in ISOLA, if such models are available.

The waveform agreement between observed and synthetic seismograms is quantified by their *correlation* (corr) or by *variance reduction* (VR): $VR = 1 - (\text{res}^2/\text{data}^2)$, where res^2 denotes misfit (i.e. the sum of squared residuals between observed and synthetic data), while data^2 is the sum of squared observed data. The two measures are related: $\text{corr}^2 = VR$ (Eq. 13 of Křížová et al. 2013). Resolution of the moment tensor is expressed by condition number (CN); it will be discussed in detail. Uncertainty of MT (including, for example, scatter plot of nodal lines, or DC% histograms) is computed from the covariance matrix of the source parameters; see Appendix of Zahradník and Custódio (2012). Stability of the inversion with respect to space position and time of subevents is tested by repeatedly removing stations, or individual components (jackknifing). The resulting focal mechanisms are checked for their agreement with polarities. Alternatively, waveform inversion can be pre-constrained by polarities (see CSPS method below).

Subevents are calculated by two methods: (i) *Iterative deconvolution* is a standard method (Kikuchi and Kanamori 1991; Sokos and Zahradník 2008). Initially, a first subevent fitting data as well as possible is found, the corresponding synthetics are subtracted from real data, then a second subevent is found, etc. Temporal variation of each subevent is that of the elementary time function. The application yields a single (best-fitting) set of subevents. (ii) *Joint inversion of source pairs* is a newer method (Zahradník and Sokos 2014), suitable if the studied earthquake seems to be basically composed of two dominant subevents. We systematically inspect all possible combinations of two trial source positions on a spatial grid, and for each member of the source pair we calculate the moment-rate function. The time function is modeled as a series of equally shifted elementary time functions whose relative weights are calculated by non-negative least squares (NNLS) (Lawson and Hanson 1974). In this way, time variation of each subevent may be considerably more complex than if it is expressed by a single elementary time function. This method yields a

suite of subevent pairs, not only the best-fitting solution. Both methods have been validated in several applications, e.g. Sokos et al. (2012), Quintero et al. (2014), Hicks and Rietbrock (2015), Sokos et al. (2015, 2016) and references therein. Each of the two methods has its pros and cons as shown by comparisons in several of the cited papers. For example, as thoroughly discussed in Zahradník and Sokos (2014), the NNLS approach may perform better for extended sources observed with imperfect station coverage. The standard iterative deconvolution seems useful for identification of variable focal mechanisms participating in complex fault ruptures. More comparisons of both methods in future would be useful.

A very difficult problem is the MT inversion of earthquakes for which only few stations can be modeled, either because the other stations are too distant, or too noisy. It is often the case of *small earthquakes*. In situations like that a special method can be used, i.e. *Cyclic Scanning of the Polarity Solutions*, shortly CSPS, combining a few waveforms at near stations with polarities at many stations (Fojtíková and Zahradník 2014; Zahradník et al. 2015). The idea is to pre-constrain the solution by means of the polarities. The polarities themselves often provide a strongly non-unique focal mechanism. Then, systematically scanning the polarity-satisfying solutions, we select among them those focal mechanisms which provide good waveform fit at the available near stations. Note that CSPS assumes 100% DC sources, because non-double-couple components of small events are rarely reliable.

ISOLA is an “all-in-one” package, containing many mutually coupled Fortran codes for computer speed and hundreds of Matlab codes, forming a compact Graphic User Interface (GUI) for user’s comfort. Its great advantage over other existing MT codes is that it combines all necessary tools for processing input data and output results, such as, for example (Fig. 1):

- Converting records from several standard seismic formats
- Defining parameters for instrumental correction
- Removing instrument response (instrumental correction)
- Calculating signal-to-noise ratio
- Trying several filters to find the usable frequency range
- Visually checking the records to avoid instrumental disturbances
- Rotating horizontal components (if not recording N, E)
- Preparing velocity models in ISOLA format and plotting them
- Choosing various geometries of trial source positions
- Calculating (full-wave) Green’s functions
- Inverting for MT in several modes (full, deviatoric, DC-constrained)
- Choosing station-dependent frequency ranges
- Selecting/de-selecting stations or their components for inversion
- Simulating waveform data (forward problem), e.g. for synthetic tests
- Visualizing space and time variation of the correlation between real and synthetic seismograms
- Plotting waveform fit, beachballs and polarities
- Plotting space-time distribution of subevents

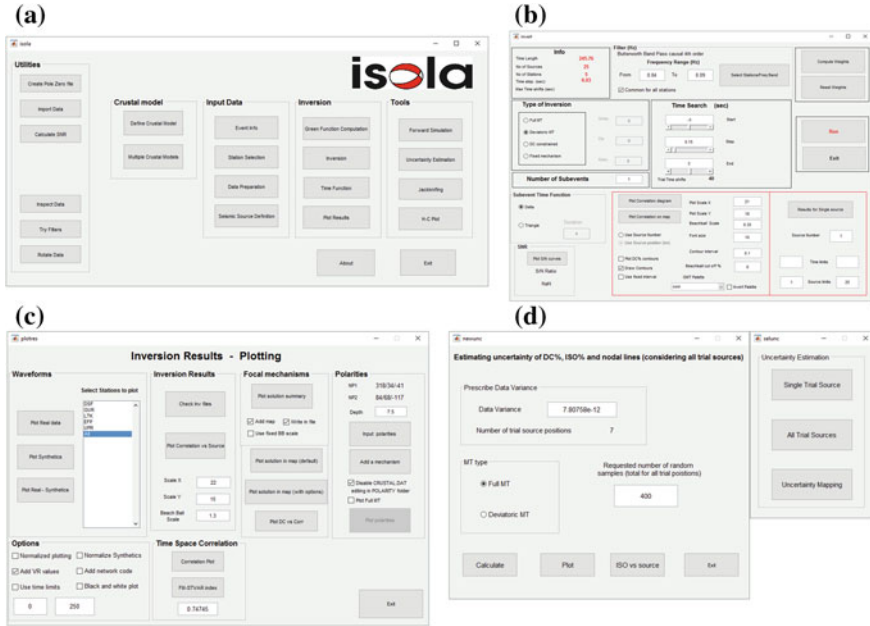


Fig. 1 An example of a few screenshots of the ISOLA GUI. **a** The front window—basic panel, **b** inversion, **c** plotting, **d** uncertainty analysis. Many other capabilities are available

- Plotting time functions
- Plotting uncertainty measures (e.g. suites of nodal lines, histograms of DC% and ISO%)

ISOLA will be preferred by users who like easy and intuitive GUI. The GUI environment is not just substitute for editing files; it is a complex system controlling all processing steps in a sophisticated way which reduces risk of many errors. Indeed, it provides an internal check (invisible to user) of consistency of the files; output files from some operations are easily used as input for the others. If batch files are needed, they don't need to be written by user, but they are automatically created by the GUI. Many warning messages and 'hints' are available. All (intermediate and final) results come in form of plots, in an almost publication-ready quality.

ISOLA is particularly useful for getting a deep insight into all processing steps and for recognizing possible variability (uncertainty) of the results. As such this software is best suited for a detailed investigation of selected earthquake sequences; for example—calculating a multiple-point source model for a mainshock, and single-point source MT solutions for largest aftershocks.

Although routine “manual” processing of many events, in a single-point source mode, by ISOLA takes place at several national seismological centers (e.g. in Greece, Turkey, Iran, Colombia, Romania), it is likely that routine processing will be better solved in future by fully automated codes. The existing automated codes, closely

related to ISOLA, are two: SCISOLA, which is a SeisComP implementation by Triantafyllis et al. (2016), and Bayesian ISOLA of Vackář et al. (2017). The latter makes use of the data covariance matrix derived from real pre-event noise, which automatically identifies and suppresses noisy components and noisy frequency ranges.

ISOLA users might be surprised why so much attention is paid to various uncertainty measures. It is because checking the resulting MT's and multiple-point source solutions, as much as possible, is of fundamental importance. A great *danger* is that ISOLA will (always) provide “some” solution, but sometimes the solution may be *physically meaningless*, and it is upon the user to detect low reliability of the results by means of all available tools of this package. This task is far from being trivial. This topic will be thoroughly discussed throughout the whole text. Some practical hints can be found at the end, in the section on ‘Frequently asked questions’.

Technical aspects, such as installation of the code, as well as the role and usage of the individual ‘windows’ of the Matlab GUI, are explained in ISOLA manual (Zahradník and Sokos 2016). The manual also contains fully documented test examples (input and output data) helping user to understand all practical use of the code. As with any code, certain training is of course invaluable. That is why very popular ISOLA training courses have been organized by various institutions, e.g. in Costa Rica (2011 and 2016), Brazil (2013), Colombia (2013), Turkey (2014). Due to these courses, many interesting international collaborations have been established.







3 Short Outline of Theory

This paragraph mainly serves as definition of the terms and quantities used in ISOLA. For complete theory, see Chap. 4 of Aki and Richards (2002). Let us start with assuming a point source (a vectorial position \mathbf{x}), a set of stations (position \mathbf{y}) and a 1D velocity model. Further we select 6 *elementary moment tensors*, $i = 1, 2, \dots, 6$. In literature, there are various sets of the 6 tensors, cf. Kikuchi and Kanamori (1991) or Bouchon (1981); we use the latter (Eq. 2 of Křížová et al. 2013). The first five tensors represent double-couple mechanisms, while the 6th one represents a pure volume change. See Table 1.

Temporal variation of the moment rate is assumed to be known, e.g. delta function. For each source-station combination (\mathbf{x}, \mathbf{y}), and a certain frequency band, we calculate 6 three-component *elementary seismograms* $G_i(\mathbf{x}, \mathbf{y}, t)$, $i = 1, 2, \dots, 6$; each one is a convolution of Green’s tensor and elementary moment tensor. For simplicity, notation of their 3 components (N, E, Z) and discretized time samples is omitted.

Seismogram due to *arbitrary moment tensor* is a linear combination of the elementary seismograms, i.e. $d(\mathbf{x}, \mathbf{y}, t) = \sum_1^6 a_i G_i(\mathbf{x}, \mathbf{y}, t)$, where the a_i coefficients have unique relation to the moment tensor and scalar moment M_0 (Eqs. 3 and 4 of Křížová et al. 2013). In matrix notation, $\mathbf{d} = \mathbf{G} \mathbf{a}$, where \mathbf{d} is a column vector of N waveform values (all stations, each one in three components, all time samples), \mathbf{G} is a $N \times 6$

Table 1 Six elementary moment tensors used in ISOLA

No.	strike (°)	dip (°)	rake (°)	
1	0	90	0	
2	270	90	-90	
3	0	90	90	
4	90	45	90	
5	0	45	90	
6	-	-	-	

matrix whose columns are G_1, \dots, G_6 (each one ordered in same way as \mathbf{d}), and \mathbf{a} is a column vector of the above introduced 6 a-coefficients.

The moment-tensor (MT) determination is a *linear* inverse problem in which \mathbf{d} represents a given (measured) data vector, \mathbf{G} is a known (numerically calculated) matrix, and \mathbf{a} is a parameter vector of 6 components to be found. A special case arises if assuming $a_6 = 0$, i.e. vanishing volume change; then we consider only 5 parameters a_i , $i = 1, 2, \dots, 5$, and 5 elementary seismograms G_1, \dots, G_5 ; this is the so-called deviatoric MT inversion. In most of practical applications $N \gg 6$, so $\mathbf{d} = \mathbf{G} \mathbf{a}$ is an over-determined linear system of algebraic equations. Optionally, a non-linear constraint is applied in ISOLA to make determinant of MT close to zero, i.e. enforcing MT to represent a pure double couple (DC). This is called DC-constrained MT inversion, particularly useful for modeling complex tectonic events as possibly composed from pure-shear subevents.

The over-determined system $\mathbf{d} = \mathbf{G} \mathbf{a}$, resulting from the waveform inversion, is inconsistent, i.e. it has no exact solution. An approximate solution can be found by the least-squares method, i.e. $\mathbf{a} = (\mathbf{G}^T \mathbf{G})^{-1} \mathbf{G}^T \mathbf{d}$, provided the inverse matrix $(\mathbf{G}^T \mathbf{G})^{-1}$ exists; here T denotes transposition and -1 stands for matrix inversion. Equivalent condition is that the $\mathbf{G}^T \mathbf{G}$ (square) matrix is regular, i.e. it has a non-zero determinant. The determinant is zero valued if one of the singular values of matrix \mathbf{G} is zero. In practice, this is almost never the case, but some singular value may be ‘small’ (in some relative sense).

Ratio of the largest and smallest singular values w of matrix \mathbf{G} is called condition number, $CN = w_{\max}/w_{\min}$. The CN can be easily calculated by means of eigenvalues e_{\max}, e_{\min} of matrix $\mathbf{G}^T \mathbf{G}$: $CN = \sqrt{e_{\max}/e_{\min}}$. Small e_{\min} , i.e. large CN value, signalize that the problem is ill-conditioned; thus the MT cannot be reliably resolved. A situation like that often appears if only few stations are available (e.g. 1 station) and/or sources are very shallow. At shallow depths some MT components are poorly resolved because the related Green’s function components are vanishing at the free

surface (Henry and Das 2002). Typically, mainly non-DC components of moment tensor suffer from the limited resolvability, i.e. those components of the earthquake moment tensor are most uncertain. A closer insight into resolvability of the linear MT inversion problem is provided by covariance matrix of model parameters $\mathbf{cov} = \sigma^2 (\mathbf{G}^T \mathbf{G})^{-1}$, where σ^2 is the data variance. Having some moment tensor retrieved in the inversion process, that MT is understood as a statistical ‘mean’. The covariance matrix allows estimation of a possible variability around the mean. Therefore, we generate random ensemble of moment tensors corresponding to the multivariate normal distribution described by the mean and covariance matrix. The obtained ensemble then, serves for constructing histograms of the parameters of interest, e.g. strike, dip and rake angles (hereafter *s/d/r*), DC%, ISO%; also, scatter-plots of possible nodal lines can be generated easily in the uncertainty tool of the GUI. In ISOLA we must assume some value of σ^2 , same for all stations. In more sophisticated methods, σ^2 is derived, either from noise (Vackář et al. 2017), or from assumed imprecision of velocity models (Halló and Gallovič 2016). Therefore, our uncertainty analysis is meaningful only in *relative* sense, like this: Assuming a fixed σ^2 value and comparing \mathbf{cov} , or CN, for several source-station configurations, several velocity models, or several frequency ranges we compare their MT resolvability. No observed waveform data are needed for this analysis, just the \mathbf{G} matrix. Note that an ill-posed waveform inversion problem (typically $\text{CN} > 10$) may have a very good match between data and synthetics, e.g. $\text{VR} = 0.9$, but such a good match in no sense guarantees that the focal mechanism is correct.

Having obtained a MT, ISOLA makes its traditional decomposition and calculates the so-called percentages of Double Couple (DC), Compensated Linear Vector Dipole (CLVD) and Isotropic component (ISO) (Eq. 8 of Vavryčuk 2001). As mentioned above, any departure from high DC (close to 100%) is to be considered with great care, because it may be a pure artifact. On the other hand, from practical point of view, it is important that if same data are processed in the full-, deviatoric-, or DC-constrained mode, featuring very different CLVD and ISO, their strike/dip/rake angles are often very similar. This indicates that the DC-part of the solution is fortunately robust.

Inaccurate knowledge of the source position is solved by repeating the linear MT inversion in a grid of predefined (trial) source positions, searching for the best-fitting centroid position and time. The MT uncertainty at the best-fitting source position is evaluated using \mathbf{cov} matrix (explained above). Alternatively, to include also effects of the uncertain source position, we make random sampling of the total MT probability density function by properly combining samples from all trial positions (Eq. 7 of Vackář et al. 2017).

Using ISOLA for retrieving more than a single subevent, and/or a more complex temporal variation of the source, needs a more detailed explanation. We briefly explain two methods currently used in the GUI, i.e. iterative deconvolution and NNLS method.

Iterative Deconvolution. The observed waveforms d (i.e. seismograms $d(t)$ in a set of stations) are represented by a sum of K point source synthetics, $d = s_1 + s_2 + \dots + s_K$. Each synthetic is due to a different source position, time, and moment

tensor which have to be found. However, all moment tensors have the same temporal variation (given by the assumed elementary time function $E(t)$, e.g. delta function). The K subevents are searched *successively*. In the first step, the entire wavefield d is optimally approximated exclusively by the first point source. The position and time of the first subevent is grid searched, while moment tensor is calculated by the least squares. As a rule, the first calculated subevent has the largest moment. The synthetic seismograms s_1 are subtracted from the data, i.e. ‘new data’ is obtained $d_1 = d - s_1$. Next inverted waveform is d_1 , thus second subevent is obtained, its contribution s_2 being again subtracted, getting $d_2 = d_1 - s_2$, etc. Several simple hints are useful to quickly guess when to stop the iterations: (i) Subevent ($K + 1$) should not have its moment much smaller (e.g. $5 \times$ smaller) than subevent (K). (ii) The cumulative moment of the subevents should increase. If a well guaranteed value of the total moment is available (e.g. that of GCMT project, <http://www.globalcmt.org/>, last accessed in June 2017), the cumulative moment should not exceed that value. (iii) If focal mechanisms are free, and they strongly vary among subevents, these mechanisms have probably no physical meaning. Then, searching subevents with a constant (prescribed) focal mechanism may be more relevant; the mechanism obtained from a previous low-frequency single-point source model is a good choice for this. (iv) The cumulative variance reduction of subevent($K + 1$) should be reasonably greater than that of subevent(K). Statistical significance of the latter can be justified by F-test, discussed later in Box 2.

NNLS inversion. The observed waveforms, d , are again supposed to be a superposition of K point-source subevents, $d = s_1 + s_2 + \dots + s_K$. Focal mechanisms (100% DC) of the subevents are assumed to be known. Their position is either known or searched (see below). Time variation $T(t)$ of moment rate of each subevent is generally not the same; it is represented by a series of J elementary time functions $E(t)$, with constant mutual time shifts τ , i.e. $T(t) = \sum_1^J n_i E(t - \tau_i)$, the goal is to calculate the n_1, n_2, \dots, n_J (non-negative) coefficients for all K sources, i.e. $J \times K$ numbers, *simultaneously*, so that we fit real data by the sum $s_1 + s_2 + \dots + s_K$. This inverse problem is solved by the non-negative least squares method of Lawson and Hanson (1974), shortly NNLS. As a result, time function of each subevent is obtained. For extended sources, particularly interesting is the time function at centroid position, which often describes temporal complexity of the whole source process (Zahradník and Sokos 2014; Sokos et al. 2016). In ISOLA GUI we also allow for a case that position of the subevents is not known. This application, useful for large events (e.g. $M > 6$), is restricted in the current GUI to two subevents only. A grid of trial source position over fault plane is designed, and the NNLS method is repeated systematically for all possible source pairs. The output is a suite of source pairs (and their time functions) which fit observed data within a selected threshold.

All calculations in ISOLA operate with observed and synthetic seismograms band-pass filtered in same frequency range. A causal, i.e. ‘one-way’, 4th order Butterworth filter is used (code XAPIir by Harris 1990). The causal filter has been selected recently (after years of using non-causal filtration) because it avoids appearance of the filtered signal before arrival time. Thus, the causal filter simplifies processing of near stations,

whose signal arrives close to origin time, $t = 0$. By observed seismograms we mean seismograms corrected for instrument, i.e. with instrument response removed, also done in ISOLA.

4 Overview of Selected Applications

To demonstrate broad applicability of ISOLA, we review here several published studies, in which the code was used. Possible interpretation of observations featuring large *non-DC components* by a source model composed from a few purely 100% DC sources were proposed (Zahradník et al. 2008b; Adamová et al. 2009). One of very few ISOLA applications proving possible reliability of a significant ISO component was that by Křížová et al. (2013). Studies of MT uncertainties started in Zahradník and Custódio (2012). The latter paper, followed by Michele et al. (2014), represented pioneering steps, demonstrating possible *mapping of the MT uncertainty* over a geographic territory of interest, without need of any real event, similarly to commonly applied analyses of the location capabilities of seismic networks. Later, the ‘uncertainty mapping’ tool became a part of ISOLA GUI and was applied by Fojtíková et al. (2016) in their network upgrade planning.

The ability of ISOLA to successfully retrieve *multiple-point source models* from near-regional records has been tested by comparisons with finite fault slip inversions, both on synthetic and real data (Zahradník and Gallovič 2010; Gallovič and Zahradník 2011, 2012). ISOLA correctly retrieved main subevents at same places where the slip inversion identified major slip patches. It was also the case of an “extreme” application of ISOLA to the M9 Tohoku 2011 earthquake (Zahradník et al. 2011). Advantages of the joint NNLS inversion of the position and size of two sources, available in ISOLA as possible replacement of iterative deconvolution, were demonstrated for a Mw 7.1 event in Turkey by Zahradník and Sokos (2014), and then the joint inversion of the source pairs was successfully used by Quintero et al. (2014), Hicks and Rietbrock (2015). The latter is an example where the authors comprehensively used many ISOLA tools.

To list at least a few, there were several applications retrieving focal mechanisms of many events in a certain seismic region for purposes of *seismo-tectonic interpretations*: Chile, Agurto et al. (2012); Martinique region, Gonzalez et al. (2017); Turkey, Cambaz and Mutlu (2016); Karakoram-Himalaya, Hazarika et al. (2017); Greece, Serpetsidaki et al. (2010) to name a few. Numerous MT’s from some of these studies led to inversion of focal mechanisms into *stress field*. A representative example of the latter is Carvalho et al. (2016), based on relatively rare waveform inversion of eleven *microearthquakes* (Mw 0.8–1.4) in Central Brazil, where data are sparse but extremely important for understanding tectonic stresses. Application of ISOLA to such small events was made possible thanks to availability of local stations (<8 km), where frequencies as high as 2 Hz could be successfully modeled. Even smaller earthquakes (Mw 0.3) were inverted in ISOLA by Benetatos et al. (2013).

Quite a lot of efforts in development of ISOLA GUI were devoted to simple visual evaluation of waveforms, important for identifying suitable frequency range. Low frequencies are needed for MT inversions because they are less sensitive to inaccuracies of available velocity models, but the low frequency range often suffers from the low signal-to-noise ratio. For example, almost no strong motion acceleration record is usable below 0.03 Hz (except stations close to faults of very large events). Broad-band records, although featuring much less instrumental noise, may contain special *low-frequency disturbances*. The latter were intensively studied by Zahradník and Plešinger (2005, 2010); later, such disturbances (called ‘mice’) were encountered worldwide by many ISOLA users. Use of disturbed records may even damage the whole MT inversion, because these records may have very large (false) amplitudes, not obvious after band-pass filtering the records. The disturbances cannot be simply filtered out. A lot of efforts were spent on ‘cleaning’ (or correcting) records, but finally we gave up inclusion of such (unstable) tools into ISOLA. Instead, we emphasized the need to identify the disturbances, and remove the damaged records from the processing. Nowadays, this can be done either manually, or—for certain type of disturbances—also automatically Vackář et al. (2015).

ISOLA enabled us to recognize several multiple events, e.g. *earthquake doublets*. In fact, the first earthquake processed by ISOLA at all was a M6.2 Lefkada 2003 earthquake (Ionian Islands, western Greece), shown to be composed from two earthquakes, Mw 5.9 and 5.8, separated of each other in space and time by 40 km and 14 s, respectively (Zahradník et al. 2005). Interestingly, this 40-km long segment of Cephalonia-Lefkada Transform Fault, unbroken in 2003, has been silent up to 2015, when it produced a M6.4 earthquake (Sokos et al. 2016). This finding is an example of how detailed MT inversions may help in elucidating existing *segmentation of major fault zones*, and thus contribute to understanding of their future potential and seismic hazard.

For an application of ISOLA to full moment tensor study of the North Korea 2017 *nuclear test* and the associated uncertainties, the reader is referred to Liu et al. (2018).

In the following two paragraphs, some of the applications are somewhat expanded. We selected same data as in ISOLA manual (Zahradník and Sokos 2016), keeping even same names: ‘Example Greece’ and ‘Example Brazil’. While in the manual we focused on technical issues (how to run the calculations, which ‘buttons’ of the GUI should be used, what are the input/output files), here we rather demonstrate a broad range of the code capabilities, mostly those which have not yet been often published, and we emphasize physical meaning of the results.

5 Example Greece

In this paragraph we demonstrate ISOLA capabilities on an example of Lefkada Mw 6.2, 2015 earthquake in Greece, published by Sokos et al. (2016). We start from low-frequency single-point analysis. Trial sources are designed in a grid of 7×7

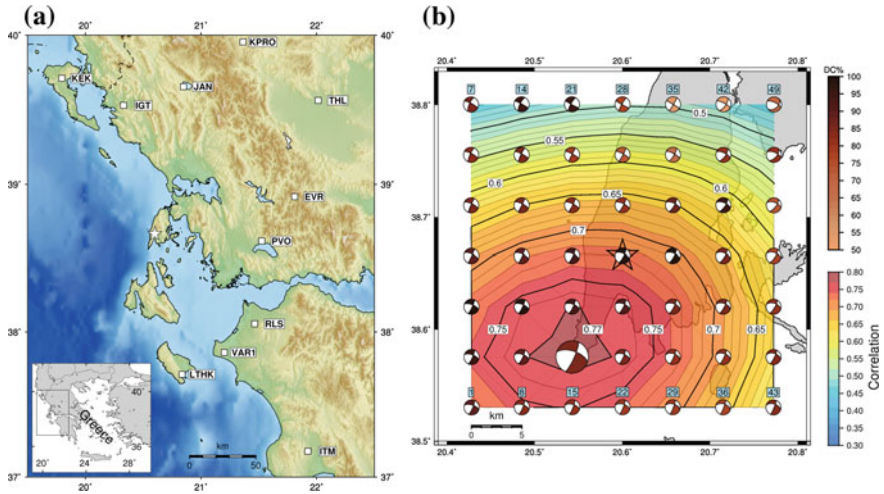


Fig. 2 Lefkada Mw 6.4 earthquake, 2015; single-point source solution. **a** Locations of the used stations (white squares). Star depicts the mainshock epicenter. Inset shows the study area with respect to Greece. **b** Grid search of centroid position, showing the Latitude-Longitude variation of the correlation between observed and synthetic waveforms for 0.01–0.05 Hz (the correlation plot). The grid is situated at a depth of 5 km. The calculated moment tensors are shown by beachballs, color-coded according their double-couple percentage (DC%). The centroid is represented by the largest beachball

points in a horizontal plane at a depth of 5 km; this depth was previously indicated by grid search below epicenter as the preferred source depth. Green functions are calculated up to $f_{max} = 0.2$ Hz, and the elementary time function is delta function.

Low frequencies, single-point source model (CMT). Initially, waveform inversion is performed in the frequency range 0.01–0.05 Hz (which we denote as “low-frequency range”, or LF). Figure 2 shows the used stations and the obtained correlation between observed and synthetic seismograms as a function of the trial source position, serving to identify the centroid position and its mechanism.

The best-fitting trial source (no. 16)—the centroid—is considerably shifted from the epicenter, 10 km towards south and 5 km towards west. This position, together with the corresponding strike, dip and rake angles (24° , 81° , -148°) constitute our CMT solution. The significant difference between hypocenter and centroid positions is due to the finite-source extent, where hypocenter (nucleation of the rupture) and centroid (center of gravity of slip on fault) are generally not the same. The centroid time is 7.5 s after hypocenter time.

Box 1: Chi-square (χ^2) test

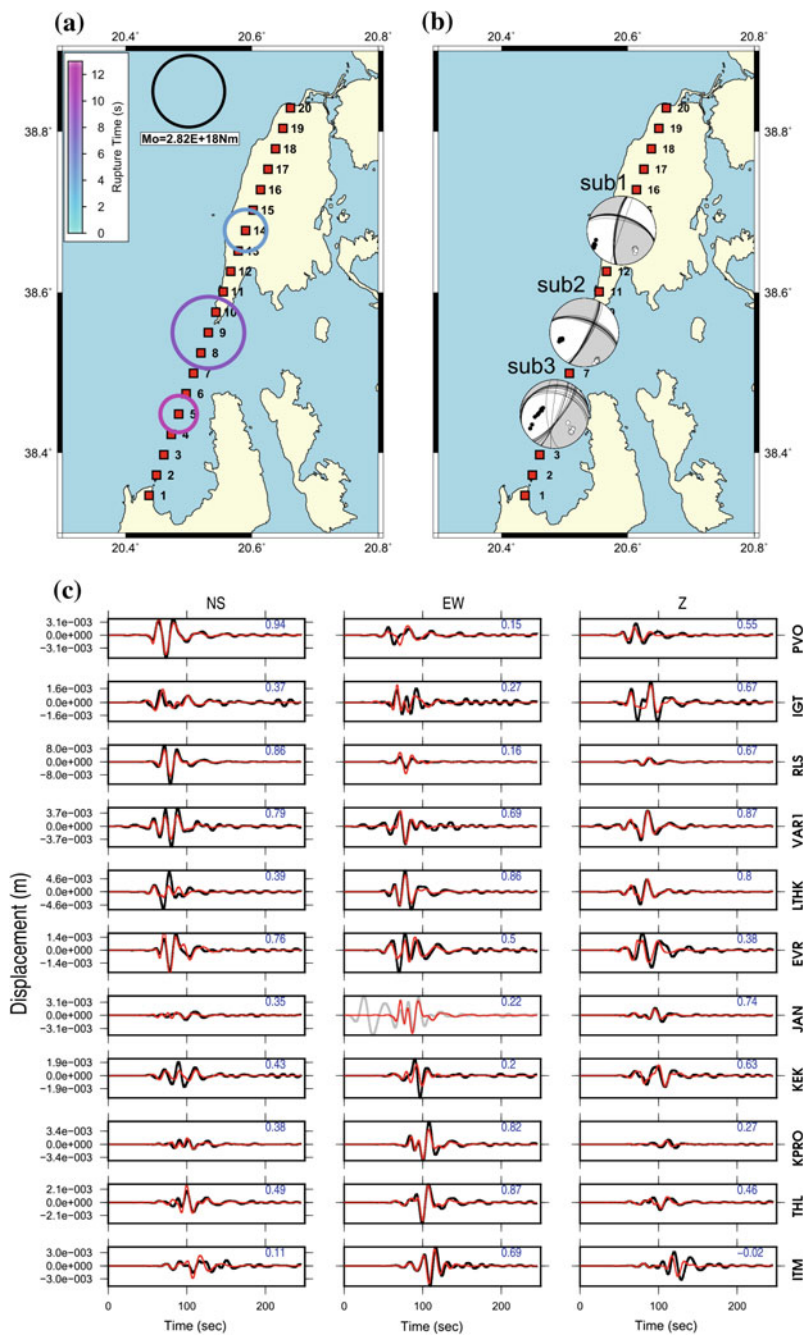
Here we explain the Chi-square test considered for possible future inclusion in the GUI. This test (Eq. 5.31 of Shearer 2009) is useful for checking statis-

tical significance of the centroid position found from the Lat-Lon correlation diagrams. Let us examine some correlation isoline, `corr_iso`, and compare it with the peak value of the correlation, `corr_opt`. The χ^2 statistic, defined as $[\text{misfit}/(\text{optimum misfit})] \times \text{ndf}$ then can be used for evaluations. The ratio of misfits can be expressed using correlations, $\chi^2 = \frac{1-\text{corr_iso}^2}{1-\text{corr_opt}^2} \text{ndf}$. Here `ndf` is the number of degrees of freedom; $\text{ndf} = N - M$, where N denotes the number of independent data and M is the number of free parameters. We take χ^2 value, and, using `ndf`, we calculate probability that the true centroid position is outside the `corr_iso` isoline.

In our example (Fig. 2b) we have `corr_opt` = 0.78 and, in the ‘red’ part of the plot we can see two isolines: `corr_iso` = 0.77 and 0.75. For these two isolines we get $\chi^2 = 149$ and 160, respectively. Now how to setup `ndf`: Due to the general fact that most temporal samples of seismogram are correlated, as a rule of thumb we consider the ‘number of data’ to be just 5 samples per component, hence 15 per station. The number 5 comes from duration of the dominant wave group, divided by predominant period (Adamová et al. 2009). Then total N can be estimated as $15 \times \text{number of stations} = 150$, while $M = 7$ (i.e., 5 MT components + 1 depth + 1 time); $\text{ndf} = 143$. Using χ^2 and `ndf`, we calculate the probability that true position of centroid is out of the 0.77 and 0.75 isoline; we obtain probability of 35% and 16%, respectively. In other words, if accepting a 35% risk of failure, we can say that the centroid is inside the 0.77 isoline. If we are more conservative, and accept only the 16% risk, then we must accept greater uncertainty of the source position, i.e. admit its position somewhere inside a broader area, especially inside the 0.75 isoline. If user is surprised by saying that one component is equivalent to just 5 data points, and believes that this number should be increased e.g. 10-times, then $\text{ndf} = 1493$ and χ^2 values increase to 1552 and 1667. Then the same isolines of `corr` = 0.77 and 0.75 correspond to probability 14% and 0.09%, and even the conservative user will claim that centroid is within the 0.77 isoline. The example demonstrated difficulties due to missing objective definition of `ndf`. Nevertheless, in both cases ($N = 5$ or 50) we see that epicenter is outside the region encompassing the likely centroid!

Although for this event, located on a well-known fault (Cephalonia Transform Fault) we know the likely fault plane (i.e. the nodal plane striking at $\sim 20^\circ$), it is instructive to use the H-C tool of ISOLA (Zahradník et al. 2008a). Considering two planes passing through centroid, and having strike and dip of nodal planes, we find that hypocenter is situated 0.5 and 6.5 km from these two planes. Proximity (0.5 km) to the plane striking at 24° is the confirmation that this nodal plane is the fault plane.

Higher frequencies, multiple-point source model. To possibly resolve more source details, we increase maximum frequency of the inversion. Now we invert waveforms in the range 0.03–0.08 Hz. Knowing that the fault was very likely related to the (almost vertical) fault striking at 24° , we design a new model, composed of trial sources distributed along a horizontal line (Fig. 3) at a depth of 5 km.



◀**Fig. 3** Lefkada Mw 6.4 earthquake, 2015; multiple-point source solution. **a** Inversion with DC-constrained focal mechanisms. Three subevents are shown by circles whose radius scales with moment and color shows a relative rupture time. The black circle at the top of the panel represents the moment scale. **b** Focal mechanisms of the subevents, jointly inverted with their position, time and moment. Jackknifing (shown by ensemble of nodal lines obtained by repeated inversions, each time removing one station) demonstrates great stability of the focal mechanism solution for the first two subevents (denoted as sub 1 and 2), and the least stability for the third one (sub 3). **c** The displacement waveform fit of the model using frequencies in 0.03–0.08 Hz band. The waveform JAN-EW is not inverted due to an instrumental disturbance; for station codes appearing at the right refer to Fig. 2a. Blue numbers indicate variance reduction of the individual components

Figure 3a, b shows the obtained 3-point source model. The waveform fit in Fig. 3c is fairly good (VR = 0.7 measured from all components but JAN-EW), perhaps except LTHK-NS, PVO-EW, ITM-Z. Misfit at KPRO-Z, ITM-NS is not much important, because weak components are always poorly fitted by least squares, if not artificially up-weighted. [Remark: Although weak components are not fitted in phase, they are usually approximately fitted in terms of their amplitude, and, in this sense, they significantly contribute to the retrieval of correct focal mechanism. That is why weak components should not be generally excluded from inversion.] The largest subevent has its position (no. 9) close to centroid. The second (smaller) subevent corresponds to a 3-s earlier moment release near epicenter (no. 14). These two subevents have similar focal mechanisms. The third (late) subevent, close to SW end of the tested line, is the smallest one, and its mechanism is different, most likely not reliable. Below we shall complement this observation by F-test.

Box 2: F-test

Similarly to Box 1, we explain here a potentially useful statistical test considered for possible future inclusion in the GUI. In relation to Fig. 3 the user can ask: Was the source composed from three episodes, or just one or two of them are significant? Statistical F-test (e.g., Menke 2012) is useful for deciding where to stop iterative deconvolution. The test needs a ratio of the L2-norm misfits from two calculations, containing n and $n + 1$ subevents: ratio = $\text{misfit}(n)/\text{misfit}(n + 1)$. The ratio of misfits needs to be compared with percentiles (critical points) of the F distribution with $\text{ndf}(n)$ and $\text{ndf}(n + 1)$ degrees of freedom, $\text{ndf} = N - M$, where N denotes the number of independent data and M is the number of free parameters. In most applications it can be assumed that $N \gg M$, $\text{ndf}(n) = \text{ndf}(n + 1) = N$. Here, as in χ^2 test, the N is estimated as $15 \times$ number of stations (i.e., 5 independent samples per component); for details, see also Suppl. Text S5 in Sokos et al. (2016).

In the present example, there is $\text{misfit}(1) = 0.0028766$, $\text{misfit}(2) = 0.0020073$, $\text{misfit}(3) = 0.0017929$. We find $\text{misfit}(1)/\text{misfit}(2) = 1.43$ and $\text{misfit}(2)/\text{misfit}(3) = 1.12$. With 10 stations, we have $N = 150$. The 0.95 critical point for 150 degrees of freedom is 1.31, while the 0.70 critical point is 1.09. Therefore

subevent 2 represents a statistically significant improvement against subevent 1 (since $1.43 > 1.31$) at the 95% confidence level, while subevent 3 is an improvement against Sub 2 at the 70% confidence level only. The latter result indicates that subevent 3 may be physically meaningless.

Similarly to Chi-square test in Box 1, we have a problem with objectively defining N . If increasing the number of independent points per component from 5 to 50 (which is still considerably less than the total number of samples per trace, 8192), N increases to 1500 and the 0.95 critical point drops from 1.31 to 1.09. This time, even subevent 3 is a statistically significant improvement compared to two subevents.

Joint inversion of waveforms for source pairs. The iterative deconvolution has revealed two subevents, the large and late at point no. 9, and the early and small at point no. 14. We want to analyze reliability of this result, to see its possible variability. In the GUI tool called Time Function (Free Source Pairs) we prescribe the fixed focal mechanism of two sources (taking $s/d/r$ angles of our CMT solution). Further, we constrain the total moment of any source pair to be the same as our previously obtained CMT moment value. The time function at every source is assumed to be composed from 12 triangles, duration 12 s each, shifted by 1 s. The result (ISOLA graphic output) is shown in Fig. 4a demonstrating various source pairs, all fitting waveforms with high VR, i.e. between 0.95 VR_{opt} and VR_{opt} , where VR_{opt} denotes the largest VR value. The plot clearly shows that it is unlikely to have the two main source contributions at positions 1–7 or 18–20. On the other hand, several combinations may exist between positions 8–17. To inspect one of the pairs, e.g. points 9 and 17, the GUI provides their time function in Fig. 4b.

6 Example Brazil

This example is related to Mw 3 earthquake which occurred in Central Brazil. In this example, we analyze a small earthquake recorded at just three near stations MR07 (37 km, 233°), MR08 (30 km, 233°), and CAN3 (84 km, 50°), where the epicentral distances and azimuths are in the brackets. Later, in the inversion, we shall use only two of them, MR07 and CAN3. It is because using both stations MR07 and MR08, situated close to each other, would be equivalent to using just one and give it weight 2 compared to the third station CAN3. There are 9 trial sources below epicenter, starting at depth 2 km, step 1 km. Green's functions (and elementary seismograms) are calculated up to 1.5 Hz. The inversion is in the range of 0.3–0.8 Hz for MR07 and 0.5–0.8 Hz for CAN3; the low-frequency limit is higher for CAN3 because frequencies <0.5 Hz were noisy.

Plot of correlation versus depth and time (Fig. 5a) indicates two strips, i.e. the bands of pink color, featuring comparable correlation values, but with flipped P-T axes. Focal mechanism corresponding roughly to origin time (which is formally

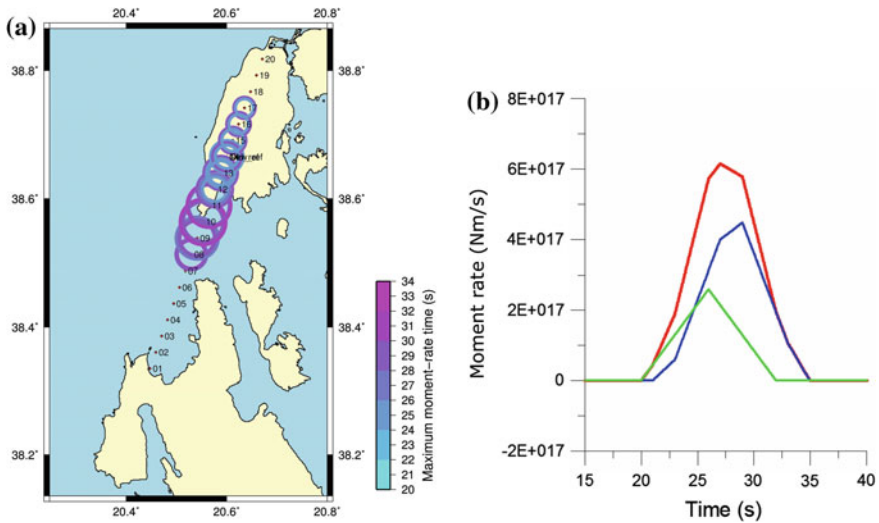


Fig. 4 Lefkada Mw 6.4 earthquake, 2015; NNLS line-source modeling. **a** An ensemble of various source pairs fitting waveforms almost equally well. The circles are sized proportional to moment and color-coded according to their rupture time (formally increased by 20 s; origin time of the earthquake is plotted as 20 s). Trial source positions 1–20 are shown. **b** The moment-rate time function for a selected source pair, that of trial positions 9 and 17, plotted in blue and green, respectively. Source rupture starts with weak early episode (green = position 17) and continues later with major moment release (blue = position 9). The total moment-rate function is shown in red

denoted as 20 s) is compared with the first motion polarities (Fig. 5b). The only strongly unfitted polarity is the compression at PMNB. Station BDFB, situated close to PMNB on the focal sphere, has an opposite polarity (discussed later). Waveform match ($VR = 0.55$) is not very good, considering that we are inverting only two stations. Also, $DC = 53\%$ is low, likely indicating a problem with velocity model. The most alarming parameter is $CN = 13$; its large value indicates poor reliability of the solution. This can be further proven by means of the Uncertainty tool: We prescribe Data Variance σ^2 equal to an estimate of posterior data variance from the previous inversion. Choosing the optimum source position 3 (corresponding to depth 4 km), the covariance matrix (Fig. 6a) shows a lot of trade-offs between the individual source parameters (a-coefficients). That is why small changes of strike/dip/rake angles, and depth, may largely tradeoff with non-DC components, producing same data fit with very different values of $DC\%$. Histogram of $DC\%$ (Fig. 6b) and the scatter nodal-line plot (Fig. 6c) confirm a poor MT resolvability.

CSPS method. To increase reliability of the focal mechanism, at least its DC-part, we apply the CSPS method. The method makes use of previous calculations in FOCMEC code of Snoke (2003) (outside of ISOLA), based on polarities at five stations MR07, MR08, CAN3, PMNB and BDFB. All of them were read from original unfiltered, uncorrected records without any doubt (clear onsets); moreover, the 3-component polarity reading confirmed their consistency with station azimuths.

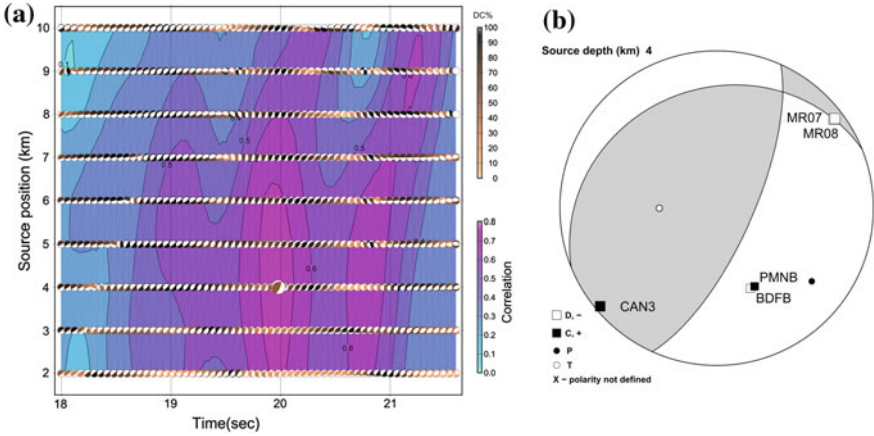


Fig. 5 Small earthquake in central Brazil. **a** Plot of correlation between observed and synthetic seismograms as a function of source depth and time. Origin time is formally placed at $t = 20$ s. The best-fitting solution is shown by the largest beachball. **b** Posterior polarity check. Two more stations are added: BDFB (distance 247 km, azimuth 158°), PMNB (602 km, 155°). The stations MR07 and MR08 overlap each other on the focal sphere, and the same takes place with BDFB and PMNB

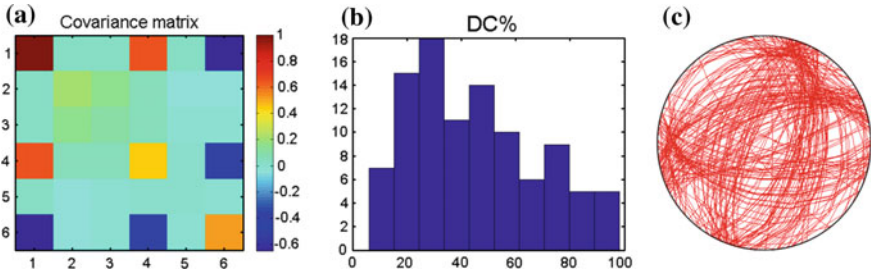


Fig. 6 Small earthquake in central Brazil—uncertainty analysis. **a** Covariance matrix for full-MT solution, numbers 1–6 refer to the inverted parameters a1–a6. Large values on the diagonal indicate the most uncertain parameters. If a column (or row) contain several large values, they indicate strong trade-off between the parameters. **b** Histogram of DC%. **c** Scatter-plot of nodal lines

Nevertheless, we ran FOCMEC with one polarity misfit allowed. It is because of the opposite polarity at stations BDFB and PMNB, which are situated close to each other on the focal sphere. If we do not allow any polarity error, a nodal line will pass between the two stations, and the FOCMEC solution would be ‘over-constrained’. Initially FOCMEC provides a set of $s/d/r$ angles and then ISOLA systematically uses all of them in waveform inversion at MR07 and CAN3 stations in a fixed-mechanism mode (100% DC); it means that ISOLA takes every strike, dip, and rake triplet, and inverts waveforms only for the source depth, time and moment. Finally, user can see not only the best-fitting solution, but also some other well-fitting (or acceptable)

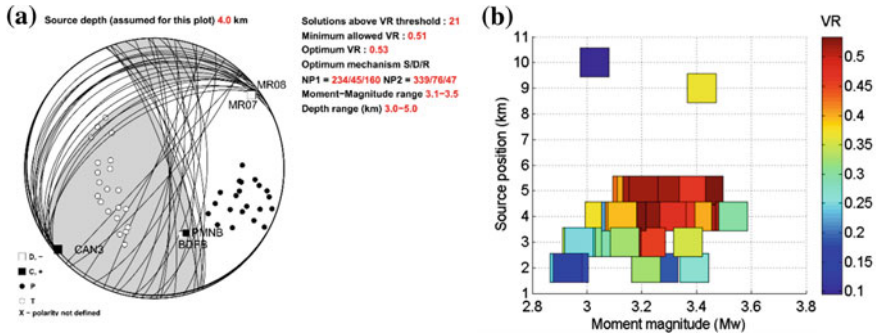


Fig. 7 Small earthquake in central Brazil—CSPS method. **a** Ensemble of well-fitting focal mechanisms obtained by waveform inversion at 2 stations, pre-constrained by polarities at 4 stations. **b** Variance reduction as a function of the source position and moment magnitude

solutions. To this goal, we define a threshold limit, to provide solutions between 0.95 VRopt and VRopt (Fig. 7a).

As seen in Fig. 7a, the combination of 6 polarities and 2 waveforms (MR07 and CAN) quite efficiently constrained the focal mechanisms. The best-fitting solution is shown by shaded sectors. It is very important to notice that this solution (as well as some others) has one nodal line passing close to stations PMNB and BDFB. It implies that their opposite polarities can be explained. As seen from Fig. 7b, available as ISOLA GUI output, the method has resolved well the depth (3–5 km) and provided $M_w = 3.1$ –3.5. This is advantage of the CSPS method, because FOCMEC method does not provide any magnitude estimate.

7 Frequently Asked Questions; Warnings

There are certain critical issues which might severely degrade ISOLA results. Some of them are discussed here.

Why sometimes strange (spurious) signals appear during processing? Many users are trying to use records whose *start time* is greater than origin time. As an example, we can imagine old triggered strong-motion acceleration records. We strongly discourage such an attempt. ISOLA automatically processes data starting at origin time ($t = 0$) and if there is a gap between $t = 0$ and (later) start time, this gap is filled with zeros; thus, spurious signals can be generated at $t = 0$ and/or at the start time. ISOLA issues a warning for such zero padding.

Sometimes, spurious signals are generated at $t = 0$ even if the start time of the record is smaller than origin time. This is often the case when we want to use records of small earthquakes and the low-frequency *noise is amplified* by instrumental correction. The spurious signal at $t = 0$ is particularly critical in case of earthquakes recorded at small epicentral distances, where the seismic signal is close to $t = 0$. A helpful trick is to

artificially decrease origin time in the very beginning of ISOLA processing. For example, a 20-s decrease of true origin time is equivalent to shifting the earthquake signal 20 s to the right. (User might have observed such a technical shift in some figures, e.g. in Fig. 5a.) This time, if a spurious signal appears at $t = 0$, it is far from the useful signal, hence the signal is not damaged. That is why we recommend that records always start well before origin time, e.g. 30 s. Another, even much simpler possible trick is to apply a pre-filter to the instrumentally corrected signals, if they suffer from large low-frequency noise. The latter operation is non-standard and only approximate; users may request some help from the authors.

Some spurious signals in the initial part of records may appear also due to improper (too short) *time window* selected for processing in ISOLA. The time window (same for all stations) must be as large as to encompass complete waveform at the most distant station. If not, later parts of the signal appear, due to temporal aliasing effect, in the initial part, i.e. between origin time and the first arrival.

Spurious signals might appear also at the *end of record*. That is why we recommend that records always end after the time window used in ISOLA.

Low-frequency disturbances ('mice', or 'flings'), already mentioned above, can be regarded as spurious signals, too (Zahradník and Plešinger 2010; Vackář et al. 2015). Use of disturbed records may damage the whole MT inversion, because these records may have very large (false) amplitudes, not obvious after band-pass filtering the records. That is why quality control of waveforms, before entering ISOLA, is extremely important. The disturbances may often be easily recognized if full-band records (without any filtration), without instrumental correction, are baseline corrected and integrated.

All components with spurious signals must be removed from inversion. Contrarily, the sole fact that some components or whole stations cannot be matched in the inversion is not indicative enough for their removal (de-selection) from the inversion!

Why observed waveforms cannot be matched? Spurious signals (discussed above) are the most frequent cause. Another typical problem is that some users do not know very well the *instrumental parameters* (poles, zeros, normalization constant, conversion from counts to m/s), or make mistakes in their use. ISOLA needs the constants in rad/s, not in Hz as provided by some instrument manufacturers. The response provided to ISOLA must be always response of the instrument for input *velocity*. The latter applies to processing of any records, i.e. those from short-period, broad-band or strong-motion instruments. For technical details of this type, the reader is referred to Appendix of the ISOLA manual (Zahradník and Sokos 2016).

In regions where seismicity is infrequent, and/or networks are sparse, the analyzed events may have severely *biased epicenter*. At the same time, having only few waveforms, the ISOLA tool for horizontal grid-searching of the source (like in Fig. 2b) may be inefficient tool for correcting the inaccurate epicenter. This drawback can be often recognized if waveforms cannot be fitted in any frequency range and with any velocity model.

Similar situation—impossibility to match real data—may occur if the stations are few, and some of them have a *gross error in instrumental parameters*. The latter can be identified by a trick: Inverting each station separately, which of course is

not reliable for MT, can provide the M_w value much greater for some stations than for the others (e.g. M6 instead M4); thus, we may get indication of a problematic instrumental gain.

Velocity models used in ISOLA may be critical. If synthetic waveforms are considerably 'shorter' than real, i.e. the synthetics miss many later arriving phases present in real record, it is an indication that velocity model is lacking relatively shallow subsurface layer(-s) of low velocity. This is often the case if velocity models used in ISOLA were derived from travel times, they provide location with relatively low travel-time residuals, but may fail in explaining waveforms, especially their surface waves. Models previously tested for agreement with surface wave dispersion are usually better. In any case, repeated ISOLA runs with *several velocity models* are always useful for checking stability of the results.

Users often worry about *Q-factors* (attenuation). ISOLA is basically 'low-frequency method'. In most applications, we work at frequencies below ~ 0.1 Hz. In this range, waveforms are less sensitive to Q; as such, $Q_p = 300$, $Q_s = 150$ in the whole crust can be usually used.

A typical mistake is that user overestimates the accuracy of his/her hypocenter depth and searches centroid in a *narrow range*, but with an unnecessarily fine grid. For example, having location depth 10 km, some users seek source in ISOLA using trial depths 9.5, 9.6, ..., 10.5 km. Instead, we must inspect a broader range of trial depths, possibly with larger steps, e.g., 5, 7.5, ..., 15 km. The same applies for temporal grid search.

MT inversion in ISOLA is solved by the least squares. This method, implicitly, fits larger amplitudes better. That is why some stations (or certain station components), having small amplitudes, are not fitted very well. This is normal situation, and there is *no reason to remove weak-amplitude components* from inversion. Even if fitted only roughly, in terms of amplitude, these components significantly contribute to the retrieval of correct focal mechanism. The problem of poorly fitted small amplitudes at some stations might be solved, to some extent, by implementing certain weighting (either using Compute Weights in the Inversion window, or by manually editing allstat.dat file in the invert folder); however, we cannot generally recommend it.

A special case arises when a single station is very near, e.g. at the epicentral distance of 10 km, while the others are at 100–300 km. In case like that, it is always recommended to make inversion both with and without the near station; it is in fact equivalent to a user-defined weighting (i.e. down-weighting the near station due to its very large amplitudes). Nevertheless, it is useful to keep such station in the analyzed station set, which means that synthetics are predicted for this station, although the station is not inverted. The *near station* may bias the inversion not only because of its large amplitude, but also because, in case of larger event, it may be affected by source finiteness (if the epicentral distance is smaller than the fault size). Another potential problem with the nearest station is that it is most vulnerable to the epicenter error. On the other limit, as regards the most *distant stations*, they are usually matched the worst; it is because the effects of the inaccurate velocity model increase with distance. As a rule, poorly fitted distant stations can be removed from inversion almost without any effect upon the solution.

A near station may help to reveal a problem with inaccurate epicenter position. To this goal, it is recommended to read the first-motion *polarities on all three components* and to check if they are consistent with azimuth of the station. Alternatively, if epicenter is correct, this check may reveal a problem with *non-precise orientation of horizontal sensors*.

Naturally, user cannot expect that all first-motion polarities will be always well predicted by the retrieved MT. Some polarities are simply not matched because they were read from noisy records, i.e. those polarities themselves were not guaranteed. Only very clear, possibly sharp impulsive onsets should be used. Unfortunately, this is rarely the case of the Moho-guided (head) waves. Some polarities are well guaranteed, but their projection on focal sphere is problematic due to inaccurate takeoff angles in imprecise velocity model. Note that takeoff angle is a high-frequency, ray-theory concept; as such, it is vulnerable to departures of real Earth from simple 1D velocity models; more vulnerable than the low-frequency waveform inversion. For example, highly unlikely are takeoff angles of very shallow sources calculated at distant stations as head waves due to shallow discontinuities (e.g. at 2 km), simply because shallow discontinuities are strongly laterally variable. Many polarity mismatches can be explained if the takeoff angles are understood as uncertain (Zahradník et al. 2015). Another possibility is to treat the polarity agreement/disagreement in statistical sense (Dias et al. 2016).

How to choose the inverted frequency band? Choosing proper frequency range for the inversion is an important issue. Theoretically, low frequencies are more welcome because synthetics are less suffering from *inaccurate velocity model*. High frequencies are welcome because they help to get more source details (e.g. to construct a multiple-point model). These two requirements must be properly balanced. In practice, the low-frequency limit is given by *natural or instrumental noise*. For example, for magnitude ~ 6 at regional stations, the signal amplitude is usually well above the noise at frequencies > 0.01 Hz, but for magnitude ~ 2 at local stations we need to start inversion perhaps at 0.5 Hz. The high-frequency limit is given by the epicentral distance. Indeed, as a rule, due to inherent inaccuracy of common velocity models we cannot model waveforms at epicentral distances greater than 10 MSW, where MSW is the minimum shear wavelength. Considering standard shear wave speed in the crust of 3 km/s, then at 0.1 and 1.0 Hz we have MSW = 30 and 3 km, respectively. Therefore, for magnitude ~ 6 we can make inversion up to 0.1 Hz at stations with epicentral distances less than 300 km. However, using frequencies up to 1 Hz we must restrict the inversion to the stations at distances less than 30 km. These numbers should be considered as a rough estimate only. Each case needs a careful consideration, or repeated tests in various frequency ranges and several velocity models.

Applying the above discussed rules, it may happen that user disposes just with a very *narrow interval* of usable frequencies. As an undesired consequence, the correlation diagrams (e.g. in Fig. 5a) have several parallel bands, or ‘*strips*’, characterized by almost same correlation values, but the strips have *flipped P-T axes*. Which mechanism is the correct one? To answer the question, the MT solution must be complemented by a polarity check, at least in few stations, optimally those which

are situated close to centers of the positive/negative sectors on the focal sphere. If the solution disagrees with polarities, user has to select the other strip, even if it has a (slightly) lower correlation. To this goal, he has to repeat the inversion, narrowing the temporal grid search so that the code identifies the ‘correct’ strip. However, if the ‘correct’ strip is far from origin time, e.g. >10 s, we have an indication that velocity model is inaccurate, and the procedure may be inapplicable.

How many stations are needed to get a reliable MT? There is *no simple answer* to this simple question. Sometimes, correct strike, dip, and rake angles are obtained even with very few stations, e.g. two, or just one. Cases like that should however be considered as ‘especially favorable’. In no way user can believe that the single station solution is correct just because it matched observed records with large variance reduction, e.g. 0.9! Getting large VR for few records should not be a problem, but it does not guarantee correct mechanism. The question why a solution obtained from few stations is good or not is partially answered by condition number. A rule of thumb is that if CN is larger than 5 or 10, the problem is ill-posed, hence the solution may be wrong. Fortunately, a wrong solution is often indicated by the overall instability of the solution, e.g. in the jackknifing tests, or in correlation graphs. That’s why the latter have been supplemented by various stability indices (FMVAR, STVAR, introduced in Sokos and Zahradník 2013). The indices should be also used with caution, because they are somewhat dependent on the subjectively chosen extent of the space-time grid. The indices have always a good sense when comparing two inversions in the same space-time region, particularly in such a case where two or more strips of high correlation are avoided (see paragraph above).

Although we said that few stations might be dangerous, ISOLA *does not need a very good azimuthal coverage*, especially if velocity models are highly reliable. The latter might be the case of the velocity models fitting well various data sets in the studied region, including travel times, dispersion curves, etc. Dense azimuthal coverage is needed in methods using less information from the records, e.g. peak P and S amplitudes, or ratios, like in FOCMEC; use of waveforms may be less demanding. Anyway, as in any physical problem, more data are always welcome (although bringing often more complications). As in many previous places we again emphasize that especially for non-DC components, extremely good data are needed.

How relevant is the moment magnitude M_w of ISOLA? The moment magnitude M_w is calculated from scalar moment M_o by standard formula (Hanks and Kanamori 1979). Hence the quality of M_w depends on M_o . So how good is our M_o ? As explained in the theoretical section, ISOLA calculates M_o from moment tensor (as its norm). The moment tensor is calculated by the least-squares method; therefore it can be shown that M_o is equal to scalar product between observed data o and synthetic data s , where s are determined for unit moment; symbolically, $M_o = (s.o)/(s.s)$, see Eq. (9) of Zahradník and Gallovič (2010). Therefore, M_o is proportional to $s.o$, which is the zero-lag correlation. If o and s are matched perfectly (except a multiplicative constant), $o = \text{const}.s$, then obviously, we correctly retrieve $M_o = \text{const}$. On the other hand, if s and o are not well correlated (not matching their waveforms), then $s.o$ is low, hence also the moment M_o is low.

Naturally, wrong M_0 may also appear either due to wrong velocity model and/or wrong depth. Indeed, considering for simplicity only S waves, M_0 is proportional to the product $\rho \beta^3$ at the assumed source depth, where ρ is density and β is the shear velocity. As a rule, seismic data are insensitive to density, but, in this sense, M_0 is an exception. If user does not know anything about density, ISOLA GUI is assisting during preparation of the ‘velocity model’, by providing an empirical formula (e.g. Talwani et al. 1959) to convert P-velocity α (in km/s) into density ρ (in g/cm³): $\rho = 1.7 + 0.2\alpha$. The only goal is to avoid some totally inappropriate values of ρ .

Is Green’s function calculation free of any problem? Fortunately, just quite rarely user might encounter numerical problems in calculating Green’s functions. These may appear as various spurious impulses, sometimes related to $t = 0$ or $t = TL$, where TL is the considered time window length. The problems may appear if sources are very shallow, e.g. < 1 km, mainly if at the same time the velocity model features very low velocities below the Earth surface, e.g. $\beta < 2$ km/s. Some of the problems can be solved by changing the internally defined parameters of the discrete wavenumber method, which is a non-standard operation. User should ask the authors for special help. Greens’ function in ISOLA cannot be calculated for zero source depth.

Why ISOLA includes the Forward Simulation tool? From time to time, users need *synthetic tests*. They want to generate synthetic data (by prescribing a given moment tensor), perhaps add some noise, and invert these data with the intention to understand the resolution of their problems. Users often forget that synthetic data without noise must be inverted with extremely good match, e.g. $VR = 0.99$, or 1.0. If obtaining $VR = 0.9$, which is a high value when processing real data, such VR is too low in synthetic noise-free inversion, and it signalizes a problem. Very often the problem is due to inappropriate preparation of the synthetic data, in particular due to certain filtering. Optimally, synthetic data must be prepared without any filtration, i.e. in a range starting at zero frequency, and ending at Nyquist frequency (or at least at a frequency much greater than f_{max} frequency of the Green function).

User may want to compare the inversion result with a solution of some agency. Although he/she can use the fixed-mechanism inversion mode, that mode does not enable use of a given (prescribed) scalar moment M_0 (hence also M_w). Prescription of complete focal mechanism, including M_0 , is possible in the forward simulation tool of ISOLA. A great advantage is that the tool makes it possible to calculate synthetics for an *arbitrary full moment tensor*, chosen by the user, e.g. a pure volume change. Moreover, in contrast to inversion (which is always made in displacement), we may choose to forward-simulate velocity.

Another reason for using forward simulation is to get a feeling how much seismograms can vary due to change of the *velocity model*.

Still another reason is curiosity to see low-frequency waveform features, missing or obscured in real data due to limited instrumental frequency band, or due to noise. In particular, it is interesting to learn about near-field effects present in low-pass synthetics, such as ‘ramps’ between P and S onsets, and/or static displacements. If the latter is significant (of the order of centimeters, or more) it signalizes usefulness to complement the seismic analyses by GPS or InSAR geodetic data.

Miscellaneous: Some ISOLA tools, very useful in certain applications, might be totally *misleading* in others. A typical example is the so-called H-C tool; Zahradník et al. (2008a). It serves for identifying fault plane among the two nodal planes. It is intended for events of $M > 5-6$, where centroid and hypocenter position might be displaced of each other at a distance considerably greater than their own errors. Then the tool may correctly identify that plane, passing through centroid, which encompasses hypocenter, so that plane is the fault. However, when using the method for weak events in situations where there is no physical reason for having centroid significantly displaced from hypocenter, and/or their errors are large, the method is naturally misleading.

ISOLA is not intended for routine use of stations at distances >1000 km, where *sphericity of the Earth* may be an issue for deep earthquakes. However the problem can be overcome (Zahradník et al. 2017), please ask authors for special help.

At the end, we would like to acknowledge the fact that many beginners are able to start with ISOLA quite intuitively, without reading any instruction. However, this is *not* the best practice, and users like that often need to solve unnecessary complications. Most complications can be avoided if putting more attention to a preliminary study. We strongly emphasize the need to read ISOLA manual and ISOLA related papers, e.g. those referenced at the end.

8 Outlook

Closely related to the problem how to find a suitable frequency range are recent efforts of Fabio Dias, Brazil. To circumvent ‘manual’ search of the range, he proposed the so-called frequency range tests FRT, where ISOLA is repeatedly used in many different ranges and results are jointly processed (Dias et al. 2016). The FRT method is a candidate for possible future inclusion in the GUI.

Statistical tools (F-test, Chi-square test), discussed in Boxes 1 and 2, but currently not included in the GUI represent other candidates.

Recent studies of small earthquakes in sparse networks that we performed in cooperation with colleagues in Argentina (Celeste Bollini) and Brazil (Juraci Carvalho) have indicated a need to solve the problem with limited applicability of a single velocity model at various stations at large epicentral distances. The solution consists in releasing strict requirement to fit waveforms (simply because we are unable to fit them). Instead, we might want to invert amplitude spectra, which are independent of unknown time shifts caused by inaccurate velocity model, or invert envelopes of the full waveforms. This study and implementation of these methods in the GUI is in progress (Zahradník and Sokos 2018).

New codes have been written also for inverting static GPS displacements into a suite of points or finite-extent sources. If several GPS observations are available for large earthquake ($M \sim 7$) near the fault, these codes might help in designing the trial point-source grids for inversion of seismic data in ISOLA.

Our plans include extension to 3D velocity models. The idea is that forward problem in 3D (Green's functions and elementary seismograms) are calculated in some finite-difference code outside ISOLA. Then it is relatively straightforward to use the 3D elementary seismograms even already in the existing ISOLA codes. Please ask for help, if you have 3D elementary seismograms and want to use them for the MT inversion of single- or multiple-point source models.

Finite-extent slip inversion is not planned for inclusion in ISOLA, because excellent codes for this purpose (Galović et al. 2015) are available elsewhere (Github: <http://fgalovic.github.io/LinSlipInv/>, last accessed June 2017). Note that the slip inversion is well applicable only to larger events ($M \sim 6$) for which we dispose with many (dozens) strong-motion records from near-fault stations.

Also not planned is automation, because this task is fully covered by SCISOLA (Triantafyllis et al. 2016), and Bayesian ISOLA (Vackář et al. 2017), already mentioned above.

Acknowledgements The authors sincerely thank to Ronnie Quintero, Lucas Barros, Patricia Pedraza and Didem Cambaz who organized ISOLA training courses. The courses provided important feedback to the authors. We also thank to users, worldwide, for huge number of e-mail questions that helped us to make the code more user friendly. ISOLA includes a modified version of the discrete-wave number code AXITRA of O. Coutant, filter XAPIir encoded by D. Harris, the NNLS inversion code of C.L. Lawson and R.J. Hanson, the MT-decomposition code by J. Šílený, several codes from Numerical recipes (Press 1992) and Matlab user file repository. Plots are created using GMT (Wessel and Smith 1998). For acknowledgment of data used as Example Greece, see Sokos et al. (2016). The Example Brazil is based on unpublished data provided by Lucas Barros and Juraci Carvalho, University of Brasilia. E.S. acknowledges financial support by HELPOS project, "Hellenic Plate Observing System" (MIS 5002697). J.Z. was supported by CzechGeo/EPOS (LM2015079) and the Czech Science Foundation (GACR-18-06716J).

References

- Adamová P, Sokos E, Zahradník J (2009) Problematic non-double-couple mechanism of the 2002 Amfilochia Mw 5 earthquake, Western Greece. *J Seismol* 13:1–12. <https://doi.org/10.1007/s10950-008-9112-4>
- Agurto H, Rietbrock A, Ryder I, Miller M (2012) Seismic-afterslip characterization of the 2010 Mw 8.8 Maule, Chile, earthquake based on moment tensor inversion. *Geophys Res Lett*. <https://doi.org/10.1029/2012gl053434>
- Aki K, Richards PG (2002) Quantitative seismology. University Science Books
- Benetatos C, Málek J, Verga F (2013) Moment tensor inversion for two micro-earthquakes occurring inside the Háje gas storage facilities, Czech Republic. *J Seismol* 17:557–577. <https://doi.org/10.1007/s10950-012-9337-0>
- Bouchon M (1981) A simple method to calculate Green's functions for elastic layered media. *Bull Seismol Soc Am* 71:959–971
- Cambaz MD, Mutlu AK (2016) Regional moment tensor inversion for earthquakes in Turkey and its surroundings: 2008–2015. *Seismol Res Lett* 87:1082–1090. <https://doi.org/10.1785/0220150276>
- Carvalho J, Barros LV, Zahradník J (2016) Focal mechanisms and moment magnitudes of micro-earthquakes in central Brazil by waveform inversion with quality assessment and inference of the local stress field. *J South Am Earth Sci* 71:333–343. <https://doi.org/10.1016/j.jsames.2015.07.020>

- Coutant O (1989) Program of numerical simulation AXITRA. University of Joseph Fourie, Grenoble, France
- Dias F, Zahradník J, Assumpção M (2016) Path-specific, dispersion-based velocity models and moment tensors of moderate events recorded at few distant stations: examples from Brazil and Greece. *J South Am Earth Sci* 71:344–358. <https://doi.org/10.1016/j.jsames.2016.07.004>
- Fojtíková L, Zahradník J (2014) A new strategy for weak events in sparse networks: the first-motion polarity solutions constrained by single-station waveform inversion. *Seismol Res Lett* 85:1265–1274. <https://doi.org/10.1785/0220140072>
- Fojtíková L, Kristeková M, Málek J et al (2016) Quantifying capability of a local seismic network in terms of locations and focal mechanism solutions of weak earthquakes. *J Seismol*. <https://doi.org/10.1007/s10950-015-9512-1>
- Gallovič F, Zahradník J (2011) Toward understanding slip inversion uncertainty and artifacts: 2. Singular value analysis. *J Geophys Res Solid Earth* 116:B02309. <https://doi.org/10.1029/2010JB007814>
- Gallovič F, Zahradník J (2012) Complexity of the Mw 6.3 2009 L'Aquila (central Italy) earthquake: 1. Multiple finite-extent source inversion. *J Geophys Res Solid Earth*. <https://doi.org/10.1029/2011jb008709>
- Gallovič F, Imperatori W, Mai PM (2015) Effects of three-dimensional crustal structure and smoothing constraint on earthquake slip inversions: case study of the Mw 6.3 2009 L'Aquila earthquake. *J Geophys Res Solid Earth* 120:428–449. <https://doi.org/10.1002/2014JB011650>
- Gonzalez O, Clouard V, Bouin M-P, Zahradník J (2017) Centroid moment tensor solutions along the central Lesser Antilles for 2013–2015. <http://dx.doi.org/10.1016/j.tecto.2017.06.024>
- Hallo M, Gallovič F (2016) Fast and cheap approximation of Green function uncertainty for waveform-based earthquake source inversions. *Geophys J Int* 207:1012–1029. <https://doi.org/10.1093/gji/ggw320>
- Hanks TC, Kanamori H (1979) A moment magnitude scale. *J Geophys Res* 84:2348. <https://doi.org/10.1029/JB084iB05p02348>
- Harris D (1990) XAPiir: a recursive digital filtering package. Lawrence Livermore National Laboratory, United States
- Hazarika D, Paul A, Wadhawan M et al (2017) Seismotectonics of the Trans-Himalaya, Eastern Ladakh, India: constraints from moment tensor solutions of local earthquake data. *Tectonophysics* 698:38–46. <https://doi.org/10.1016/j.tecto.2017.01.001>
- Henry C, Das S (2002) The Mw 8.2, 17 February 1996 Biak, Indonesia, earthquake: rupture history, aftershocks, and fault plane properties. *J Geophys Res Solid Earth* 107:ESE 11-1–ESE 11-16. <https://doi.org/10.1029/2001jb000796>
- Hicks SP, Rietbrock A (2015) Seismic slip on an upper-plate normal fault during a large subduction megathrust rupture. *Nat Geosci* 8:955–960. <https://doi.org/10.1038/NNGEO2585>
- Kikuchi M, Kanamori H (1991) Inversion of complex body waves—III. *Bull Seismol Soc Am* 81:2335–2350
- Křížová D, Zahradník J, Kiratzi A (2013) Resolvability of isotropic component in regional seismic moment tensor inversion. *Bull Seismol Soc Am* 103:2460–2473. <https://doi.org/10.1785/0120120097>
- Lawson CL, Hanson RJ (1974) Solving least square problems. New Jersey, 340 pp
- Liu J, Li L, Zahradník J, Sokos E, Liu C, Tian X (2018) North Korea's 2017 test and its nontectonic aftershock. *Geophys Res Lett* 45. <https://doi.org/10.1002/2018GL077095>
- Menke W (2012) Geophysical data analysis: discrete inverse theory. Elsevier/Academic Press
- Michele M, Custódio S, Emolo A (2014) Moment tensor resolution: case study of the Irpinia Seismic Network, Southern Italy. *Bull Seismol Soc Am* 104:1348–1357. <https://doi.org/10.1785/0120130177>
- Press WH (1992) Numerical recipes in FORTRAN: the art of scientific computing. Cambridge University Press

- Quintero R, Zahradník J, Sokos E (2014) Near-regional CMT and multiple-point source solution of the September 5, 2012, Nicoya, Costa Rica Mw 7.6 (GCMT) earthquake. *J South Am Earth Sci* 55:155–165. <https://doi.org/10.1016/j.jsames.2014.07.009>
- Serpetsidaki A, Sokos E, Tselentis G-A, Zahradník J (2010) Seismic sequence near Zakynthos Island, Greece, April 2006: identification of the activated fault plane. *Tectonophysics* 480:23–32. <https://doi.org/10.1016/j.tecto.2009.09.024>
- Shearer PM (2009) *Introduction to seismology*. Cambridge University Press
- Snoke JA (2003) FOCMEC: FOCal MECHANism determinations. In: Lee WHK, Kanamori H, Jennings PC, Kisslinger C (eds) *International handbook of earthquake and engineering seismology*. Academic Press, San Diego, pp 1629–1630
- Sokos EN, Zahradník J (2008) ISOLA a Fortran code and a Matlab GUI to perform multiple-point source inversion of seismic data. *Comput Geosci* 34:967–977. <https://doi.org/10.1016/j.cageo.2007.07.005>
- Sokos E, Zahradník J, Kiratzi A et al (2012) The January 2010 Efpalio earthquake sequence in the western Corinth Gulf (Greece). *Tectonophysics* 530–531:299–309. <https://doi.org/10.1016/j.tecto.2012.01.005>
- Sokos E, Zahradník J (2013) Evaluating centroid-moment-tensor uncertainty in the new version of ISOLA software. *Seismol Res Lett*. <https://doi.org/10.1785/0220130002>
- Sokos E, Kiratzi A, Gallovič F et al (2015) Rupture process of the 2014 Cephalonia, Greece, earthquake doublet (Mw 6) as inferred from regional and local seismic data. *Tectonophysics* 656:131–141. <https://doi.org/10.1016/j.tecto.2015.06.013>
- Sokos E, Zahradník J, Gallovič F et al (2016) Asperity break after 12 years: the Mw 6.4 2015 Lefkada (Greece) earthquake. *Geophys Res Lett* 43:6137–6145. <https://doi.org/10.1002/2016GL069427>
- Talwani M, Sutton GH, Worzel JL (1959) A crustal section across the Puerto Rico trench. *J Geophys Res* 64:1545–1555. <https://doi.org/10.1029/JZ064i010p01545>
- Triantafyllis N, Sokos E, Ilias A, Zahradník J (2016) Scisola: automatic moment tensor solution for SeisComP3. *Seismol Res Lett* 87:157–163. <https://doi.org/10.1785/0220150065>
- Vackář J, Burjánek J, Zahradník J (2015) Automated detection of long-period disturbances in seismic records; MouseTrap code. *Seismol Res Lett* 86:442–450. <https://doi.org/10.1785/0220140168>
- Vackář J, Burjánek J, Gallovič F et al (2017) Bayesian ISOLA: new tool for automated centroid moment tensor inversion. *Geophys J Int* 210:693–705. <https://doi.org/10.1093/gji/ggx158>
- Vavryčuk V (2001) Inversion for parameters of tensile earthquakes. *J Geophys Res* 106:16339–16355. <https://doi.org/10.1029/2001JB000372>
- Wessel P, Smith WHF (1998) New, improved version of generic mapping tools released. *EOS Trans Am Geophys Union* 79:579. <https://doi.org/10.1029/98EO00426>
- Zahradník J, Gallovič F (2010) Toward understanding slip inversion uncertainty and artifacts. *J Geophys Res*. <https://doi.org/10.1029/2010JB007414>
- Zahradník J, Plešinger A (2005) Long-period pulses in broadband records of near earthquakes. *Bull Seismol Soc Am* 95:1928–1939. <https://doi.org/10.1785/0120040210>
- Zahradník J, Plešinger A (2010) Toward understanding subtle instrumentation effects associated with weak seismic events in the near field. *Bull Seismol Soc Am* 100:59–73. <https://doi.org/10.1785/0120090087>
- Zahradník J, Serpetsidaki A, Sokos E, Tselentis G-A (2005) Iterative deconvolution of regional waveforms and a double-event interpretation of the 2003 Lefkada Earthquake, Greece. *Bull Seismol Soc Am* 95:159–172. <https://doi.org/10.1785/0120040035>
- Zahradník J, Gallovič F, Sokos E et al (2008a) Quick fault-plane identification by a geometrical method: application to the Mw 6.2 Leonidio Earthquake, 6 January 2008. Greece. *Seismol Res Lett* 79:653–662. <https://doi.org/10.1785/gssrl.79.5.653>
- Zahradník J, Sokos E, Tselentis G-A, Martakis N (2008b) Non-double-couple mechanism of moderate earthquakes near Zakynthos, Greece, April 2006; explanation in terms of complexity. *Geophys Prospect* 56:341–356. <https://doi.org/10.1111/j.1365-2478.2007.00671.x>

- Zahradník J, Gallovič F, Sokos E, Tselentis G-A (2011) Preliminary slip model of M9 Tohoku earthquake from strong-motion stations in Japan—an extreme application of ISOLA code. http://www.emsc-csem.org/Files/event/211414/ISOLA_Report_tohoku.pdf. Accessed 21 June 2017
- Zahradník J, Custodió S (2012) Moment tensor resolvability: application to Southwest Iberia. *Bull Seismol Soc Am* 102:1235–1254. <https://doi.org/10.1785/0120110216>
- Zahradník J, Sokos E (2014) The Mw 7.1 Van, Eastern Turkey, earthquake 2011: two-point source modelling by iterative deconvolution and non-negative least squares. *Geophys J Int* 196:522–538. <https://doi.org/10.1093/gji/ggt386>
- Zahradník J, Fojtíková L, Carvalho J et al (2015) Compromising polarity and waveform constraints in focal-mechanism solutions; the Mara Rosa 2010 Mw 4 central Brazil earthquake revisited. *J South Am Earth Sci* 63:323–333. <https://doi.org/10.1016/j.jsames.2015.08.011>
- Zahradník J, Sokos E (2016) ISOLA User's Guide, Training course in Jaco, Costa Rica, 2016, 30 pp. http://geo.mff.cuni.cz/~jz/for_ISOLA/
- Zahradník J, Sokos E (2018) Fitting waveform envelopes to derive focal mechanisms of moderate earthquakes. *Seismol Res Lett*, <https://doi.org/10.1785/0220170161>
- Zahradník J, Čížková H, Bina CR et al (2017) A recent deep earthquake doublet in light of long-term evolution of Nazca subduction. *Sci Rep* 7:45153. <https://doi.org/10.1038/srep45153>